

Uncertainty quantification in kinematic-wave models

Peng Wang¹, Daniel M. Tartakovsky*

Department of Mechanical and Aerospace Engineering, University of California, San Diego, 9500 Gilman Dr., La Jolla, CA 92093, USA

ARTICLE INFO

Article history:

Received 20 July 2011

Received in revised form 16 July 2012

Accepted 20 July 2012

Available online 7 August 2012

Keywords:

Uncertainty quantification

Random parameters

Probability density function

Hyperbolic conservation law

ABSTRACT

We develop a probabilistic approach to quantify parametric uncertainty in first-order hyperbolic conservation laws (kinematic wave equations). The approach relies on the derivation of a deterministic equation for the cumulative density function (CDF) of a system state, in which probabilistic descriptions (probability density functions or PDFs) of system parameters and/or initial and boundary conditions serve as inputs. In contrast to PDF equations, which are often used in other contexts, CDF equations allow for straightforward and unambiguous determination of boundary conditions with respect to sample variables. The accuracy and robustness of solutions of the CDF equation for one such system, the Saint-Venant equations of river flows, are investigated via comparison with Monte Carlo simulations.

© 2012 Elsevier Inc. All rights reserved.

1. Introduction

Since its development by Lighthill and Whitham [1,2], the kinematic wave theory (KWT) has been used to model a number of environmental phenomena, including overland flow, channel flow, multiphase flow in porous media, erosion and sediment transport [3,4]. It is routinely employed in analyses of urban storm-water drainage systems to route flood hydrographs [4].

The KWT theory postulates a functional relationship between a quantity $k(\mathbf{x}, t)$ and its flux $\mathbf{q}(\mathbf{x}, t)$, $\mathbf{q} = \mathbf{q}(k)$, so that a phenomenon is described by a continuity equation

$$\frac{\partial k}{\partial t} + \nabla \cdot \mathbf{q} = S, \quad \mathbf{q} = \mathbf{q}(k), \quad (1)$$

where $S(\mathbf{x}, t)$ is a source. This is in contrast with dynamic-wave models, which employ the conservation of momentum to establish a dynamic relation between $k(\mathbf{x}, t)$ and $\mathbf{q}(\mathbf{x}, t)$. For Froude numbers smaller than 1 (appropriate for flood waves), the dynamic waves (long gravity waves) do appear, but they attenuate rapidly and the main disturbance is carried downstream by kinematic waves only [1]. We use this application (overland flow in flood forecasting) to motivate the subsequent analysis. In doing so, we assume that the function $\mathbf{q} = \mathbf{q}(k)$ is invertible and treat the flux $\mathbf{q}(\mathbf{x}, t)$ as a primary state variable. If this assumption is invalid, then our approach can be applied directly to (1) in which $\mathbf{k}(\mathbf{x}, t)$ is a primary state variable (see the concluding remarks in Section 6).

When the KWT Eq. (1) is used to describe flow in long rivers, the functional relationship $\mathbf{q} = \mathbf{q}(k)$ is typically given by either Chézy or Manning formulae [4], which represent a balance between the friction at the bottom and the gravitational force. These constitutive relations are parameterized with a friction coefficient and a downward slope, both of which often exhibit high spatial variability and are usually underspecified by data. In addition to this parametric uncertainty, the source

* Corresponding author.

E-mail address: dmt@ucsd.edu (D.M. Tartakovsky).

¹ Current address: Pacific Northwest National Laboratory, P.O. Box 999, MSIN K7-90, Richland, WA 99352, USA.

function S , which represents influx from tributaries and/or runoff from the ambient terrain, as well as initial and boundary conditions are subject to uncertainty. Although data acquisition continues to improve, ubiquitous data sparsity and measurement/interpretation errors render overland flow predictions inherently uncertain. This predictive uncertainty is routinely mentioned as one of the fundamental challenges in flood forecasting [5].

A common approach to quantifying uncertainty in system parameters and driving forces is to treat them as random fields, whose statistics are inferred from available data. This renders the KWT Eq. (1) stochastic. Its solution is given in terms of probabilistic density functions (PDFs) of the system states \mathbf{q} and k , and amounts to propagation of parametric uncertainty through the modeling process.

Early attempts to quantify uncertainty in modeling predictions based on the stochastic KWT Eq. (1) dealt with spatially-averaged quantities [6–10]. Spatially-distributed probabilistic predictions were obtained by solving the stochastic KWT Eq. (1) with Monte Carlo simulations (MCS) [11,12] and stochastic finite elements [13–18]. For transient nonlinear systems such as (1) these direct approaches are computationally expensive, and often prohibitively so, especially when the parameter fields have small correlation lengths and high variances. They are typically used to compute the first two ensemble moments of system states. Accurate estimates of the tails of system states' PDFs entail further computational costs.

We present an alternative approach to uncertainty quantification in flow models based on the stochastic KWT Eq. (1). The approach is based on the derivation of a deterministic differential equation for cumulative density functions (CDFs) of the system states $\mathbf{q}(\mathbf{x}, t)$ and $k(\mathbf{x}, t)$. Our framework is conceptually similar to the PDF equations approach used to describe the dynamics of (passive or reactive) scalars in turbulent flows (e.g., [19]) and to quantify uncertainty in models of reactive transport in heterogeneous porous media [20]. Yet it offers a distinct advantage of removing the ambiguity in formulation of boundary conditions.

In Section 2, we provide a shallow-water formulation of surface flow and identify the key sources of uncertainty. Section 3 contains the derivation of a CDF equation and corresponding boundary conditions. In Section 4, this equation is solved analytically for two special cases describing flood dynamics in long rivers. We investigate the robustness and salient features of the CDF solutions in Section 5, using MCS as a benchmark. The overall conclusions are drawn in Section 6.

2. Problem formulation

2.1. Governing equations

Motion of a homogeneous fluid whose horizontal extent is much larger than its vertical counterpart can be described by the shallow water equations. It is common to use their one-dimensional form, which is often referred to as the Saint–Venant equations,

$$\frac{\partial k}{\partial t} + \frac{\partial q}{\partial x} = S, \tag{2}$$

to model open-channel flow. In this application of the KWT Eq. (1), $k(x, t)$ [L^2] denotes the cross-sectional area of a channel occupied by the fluid at a point x along the channel's length, $q(x, t)$ [L^3T^{-1}] is the volumetric flow rate, and $S(x, t)$ [L^2T^{-1}] denotes the lateral inflow rate. When kinematic waves in long rivers pass a junction with a tributary, the latter's effects on the flood movement are represented by S . The KWT Eq. (1) provides a good approximation of the flood dynamics if influence on the river upstream of the junction is neglected [1]. Since the kinematic wave approximation neglects backwater effects—the upstream propagation caused by local acceleration, convective acceleration, and pressure—the flow rate throughout the flow domain is non-negative, $q(x, t) \geq 0$ for all x and t .

For wide channels (i.e., channels whose hydraulic radius equals the depth of water), commonly used functional relations between k and q at any point x and time t (e.g., Darcy–Weisbach, Chézy, or Manning formulae) can be written as

$$q = \alpha k^{1/\beta}. \tag{3}$$

Here the parameter α represents the effects of surface slope and resistance, and the exponent β is a measure of turbulence that characterizes the flow regime as laminar, turbulent or transitional [4]. In general, both parameters can vary in space and time, $\alpha(x, t)$ and $\beta(x, t)$. Although the bed of an alluvial river varies with time [21], these changes occur on a time scale that is much larger than that of the flow, so that $\alpha = \alpha(x)$. While not strictly necessary, we assume that the exponent β is constant in order to simplify the presentation. Combining (2) and (3) gives

$$\gamma(x) \frac{\partial q^\beta}{\partial t} + \frac{\partial q}{\partial x} = S(x, t), \quad \gamma \equiv \alpha^{-\beta}. \tag{4}$$

The open-channel flow Eq. (4) is subject to the initial and boundary conditions

$$q(x = 0, t) = q_0(t), \tag{5a}$$

$$q(x, t = 0) = q_{in}(x). \tag{5b}$$

We allow the coefficient $\gamma(x)$, the source function $S(x, t)$, the inlet flow rate $q_0(t)$, and the initial flow rate $q_{in}(x)$ to be uncertain. The uncertainty is quantified by treating these functions as random fields. Within this probabilistic framework, a ran-

dom quantity $\mathcal{A}(x, t; \omega)$ varies not only in the physical domain, $(x, t) \in (0, \infty) \times (0, \infty)$, but also in the probability space $\omega \in \Omega$. Our goal is to obtain a complete (single space–time point) probabilistic description of $q(x, t; \omega)$. In the following, the dependence of the random fields on ω is suppressed to simplify the notation.

2.2. Example of statistical parameterizations

Consider, as an example of the general relation (3), the Manning formula

$$q = \frac{\sqrt{s_0}}{n} k^{4/3}, \quad (6)$$

wherein $s_0(x)$ denotes the channel slope, and $n(x)$ ($s/m^{1/3}$) is the Manning's roughness coefficient. Both $s_0(x)$ and $n(x)$ are typically uncertain and often treated as random (e.g., [22–25] and the references therein). The data reviewed in these and other analyses suggest that no single distribution is capable of capturing their spatial variability at all sites, with the normal, log-normal, gamma, logistic or log–logistic PDFs found to fit various data sets best. The spatial correlations of $s_0(x)$ and $n(x)$, and their cross-correlation, are likewise site-specific. For the data analyzed in [22], the random field $s_0(x)$ was found to be spatially uncorrelated (white noise) and either weakly correlated or uncorrelated with other hydraulic parameters.

The relevant statistics of the parameter $\gamma(x) = (\sqrt{s_0}/n)^{-\beta}$ in (4) are related to those of $s_0(x)$ and $n(x)$ in Appendix A.

3. CDF equations

We start by introducing a “raw” (or “fine-grained”) cumulative density function (CDF),

$$\Pi(Q; x, t) = \mathcal{H}[Q - q(x, t)], \quad (7)$$

where \mathcal{H} is the Heaviside step function, and Q is a deterministic value (outcome) that the random flow rate q can take at a space–time point (x, t) . Let $p_q(Q; x, t)$ denote a single-point probability density function (PDF) of q at the space–time point (x, t) . Then taking the ensemble average (over random q) of (7) yields a single-point CDF of q ,

$$\overline{\Pi}(Q; x, t) \equiv \int_0^\infty \mathcal{H}(Q - q') p_q(q'; x, t) dq' = F_q(Q; x, t). \quad (8)$$

For $q(x, t)$ in (4) and (5), its raw CDF satisfies a two-dimensional stochastic linear CWT equation (Appendix B)

$$\beta\gamma(x)Q^{\beta-1} \frac{\partial \Pi}{\partial t} + \frac{\partial \Pi}{\partial x} + S(x, t) \frac{\partial \Pi}{\partial Q} = 0 \quad (9)$$

subject to the initial and boundary conditions

$$\Pi(Q; x, t = 0) = \Pi_{in} = \mathcal{H}[Q - q_{in}(x)], \quad (10a)$$

$$\Pi(Q; x = 0, t) = \Pi_0 = \mathcal{H}[Q - q_0(t)], \quad (10b)$$

$$\Pi(0; x, t) = 0. \quad (10c)$$

The straightforward and unambiguous way in which the boundary condition (10c) is formulated provides the key advantage of our CDF method over commonly used PDF methods [19,20]. The latter are formulated in terms of “raw” PDFs, $\Pi(Q, q; x, t) = \delta[Q - q(x, t)]$, whose value at $Q = 0$ for any space–time point (x, t) is generally unknown.

The CDF formulation (9), (10) offers a number of other advantages over direct solutions of the flow Eqs. (4) and (5). First, one needs to compute (e.g., with MCS or stochastic finite elements) only the first ensemble moment of Π to obtain the full distribution of q . Second, linearity of the CDF Eqs. (9), (10) simplifies their theoretical and numerical analyses, enabling, for example, examination of the convergence and other properties of polynomial chaos methods [26]. More important for the subsequent analysis, one can take advantage of the large body of literature on stochastic averaging of linear advective transport in random velocity fields $\mathbf{v}(x, t)$,

$$\frac{\partial \Pi}{\partial t} + \mathbf{v} \cdot \nabla_x \Pi = 0. \quad (11)$$

In the context of (9), (10),

$$\mathbf{x} = (x, Q)^T, \quad \mathbf{v} = (v_x, v_Q)^T, \quad v_x = \frac{Q^{1-\beta}}{\beta\gamma(x)}, \quad v_Q = \frac{Q^{1-\beta} S(x, t)}{\beta\gamma(x)}. \quad (12)$$

Specifically, the ensemble averaging of (11) would yield an effective transport equation for the CDF of q ,

$$\frac{\partial F_q}{\partial t} + \mathbf{v}_{eff} \cdot \nabla_x F_q = \nabla_x \cdot (\mathbf{D} \nabla_x F_q), \quad (13)$$

where \mathbf{v}_{eff} and \mathbf{D} are the effective velocity and the eddy-diffusivity tensor, respectively. This equation is based on a closure approximation, but is asymptotically exact when F_q varies slowly with \mathbf{x} and t relative to \mathbf{v} [27,28].

In the present study, we consider two special cases of (9), $S = 0$ and $S = S(x)$, both of which enable one to obtain the CDFs F_q without resorting to closure approximations.

4. CDF solutions

4.1. Flood propagation in the absence of lateral inflow

The open-channel flow Eq. (4) with $S \equiv 0$ provides a classical setting first analyzed by Lighthill and Whitham [1] to model flood propagation in long rivers. The corresponding raw CDF problem (9), (10) admits an analytical solution (Appendix C),

$$\Pi(Q; x, t) = \mathcal{H}(C - t)\mathcal{H}[Q - q_{in}(x^*)] + \mathcal{H}(t - C)\mathcal{H}[Q - q_0(t - C)]. \tag{14a}$$

Here

$$C(x) = \int_0^x \beta Q^{\beta-1} \gamma(x') dx' \tag{14b}$$

and $x' = x^*$ is a solution of the equation

$$C(x') = C(x) - t \tag{14c}$$

for a given Q, x and t .

For large times, $t > C$, the general solution (14) reduces to

$$\Pi(Q; x, t) = \mathcal{H}[Q - q_0(t - C)]. \tag{15}$$

4.2. Flood propagation under steady lateral inflow

In the open-channel flow Eq. (4), the source term $S = S(x)$ might represent either input from a river's tributaries (in which case S can be treated as a sum of delta functions) or runoff (in which case S is continuous) or their combination. The corresponding raw CDF problem (9), (10) admits an analytical solution (Appendix D)

$$\Pi(Q; x, t) = \mathcal{H}(C - t)\mathcal{H}[Q - I(x, x^*) - q_{in}(x^*)] + \mathcal{H}(t - C)\mathcal{H}[Q - I(x, 0) - q_0(t - C)]. \tag{16a}$$

Here

$$C = \int_{x_0}^x \beta [Q - I(x, x'')]^{\beta-1} \gamma dx'', \quad I(x, x') = \int_{x'}^x S dx'' \tag{16b}$$

and $x' = x^*$ is a solution of the equation

$$\int_{x_0}^{x'} \beta [Q - I(x, x'')]^{\beta-1} \gamma dx'' = \int_{x_0}^x \beta [Q - I(x, x'')]^{\beta-1} \gamma dx'' - t, \tag{16c}$$

with

$$x_0 = \begin{cases} 0 & Q \geq I(x, 0) \\ \eta & Q < I(x, 0) \end{cases}, \quad I(\eta, 0) = I(x, 0) - Q. \tag{16d}$$

If $S(x) \equiv 0$, (16) reduces to (14).

4.3. CDF solutions

Expressions (14) and (16) map the random system parameter $\gamma(x)$ and driving forces $q_0(t), S(x)$, and $q_{in}(x)$ onto the raw CDF Π . To simplify the presentation, we take q_{in} to be deterministic, and analyze in detail flow in the absence tributaries ($S = 0$). This setting captures the salient features of the CDF method, and its extension to more complicated flow scenarios is relatively straightforward.

The parametric uncertainty can now be quantified by p_{γ, q_0} , a joint PDF of random inputs $\gamma(x)$ and $q_0(t)$. Since $\gamma(x)$ and $q_0(t)$ represent two different physical phenomena, they can be treated as independent, so that $p_{\gamma, q_0} = p_{\gamma} p_{q_0}$ and (8) gives rise to a CDF solution

$$F_q(Q; x, t) = \iint \Pi(\Gamma, Q_0; x, t) p_{\gamma}(\Gamma) p_{q_0}(Q_0) d\Gamma dQ_0. \tag{17}$$

The (non-Gaussian, correlated) random field $\gamma(x)$ enters (14) only as an integrand in

$$I_{\gamma}(x) = \int_0^x \gamma(x') dx'. \tag{18}$$

Table 1

Statistics of the uncertain (random) parameters. These values are representative of data in [23–25,30].

Parameter	PDF	$\rho(r)$	Mean	CV	λ
$q'_0(t)$	Normal	$\delta(r)$	0	0.1	–
$s_0(x)$	Lognormal	$\exp(r/\lambda)$	0.01	0.25	200
$n(x)$	Lognormal	$\exp(r/\lambda)$	0.037	0.25	200

Therefore, (17) can be replaced with

$$F_q(Q; x, t) = \iint \Pi(I, Q_0; x, t) p_{I_\gamma}(I) p_{q_0}(Q_0) dI dQ_0. \quad (19)$$

It remains to compute $p_{I_\gamma}(I; x)$, the PDF of $I_\gamma(x)$.

Let λ_γ denote the correlation length of $\gamma(x)$. For $x \ll \lambda_\gamma$, $\gamma(x)$ on the interval $[0, x]$ is approximately constant, $I_\gamma(x) \approx x\gamma$ and $C(x)$ in (14) can be approximated by

$$C(x) \approx \beta Q^{\beta-1} x \gamma(x), \quad x \ll \lambda_\gamma. \quad (20)$$

For $x \gg \lambda_\gamma$, $I_\gamma(x)$ becomes Gaussian with mean $x\bar{\gamma}$ and variance $2x\sigma_\gamma^2$, and $C(x)$ becomes

$$C(x) \approx \beta Q^{\beta-1} N(x\bar{\gamma}, 2x\sigma_\gamma^2), \quad x \gg \lambda_\gamma. \quad (21)$$

If $\gamma(x)$ lacks spatial correlation [22], this expression becomes exact. For intermediate x , we approximate the statistics of $I_\gamma(x)$ with the central limit theorem (CLT)-based approach [29] (see Appendix E).

Below we use a computational example to investigate the accuracy and robustness of the alternative approximations of $p_{I_\gamma}(I; x)$, and their effects on the flow-rate CDF F_q , via comparison with Monte Carlo simulations.

4.4. Computational example

We set the initial flow rate to $q_{\text{in}} = 0.5 \text{ m}^3/\text{s}$ and the flow rate at the inlet $x = 0$ to

$$q_0(t) = \bar{q}_0 \left| \sin \left(\frac{\pi t}{P} \right) \right| [1 + q'_0(t)]. \quad (22)$$

The mean flow rate $\bar{q}_0 = 1 \text{ m}^3/\text{s}$ satisfies the subcritical flow condition required for the kinematic wave approximation to be valid, and P denotes the period. The fluctuating term $q'_0(t)$ is white noise. Its statistics, as well as those of the random channel slope $s_0(x)$ and Manning coefficient $n(x)$ are summarized in Table 1, wherein CV denotes the coefficient of variation (absolute value of the ratio of the standard deviation to the mean), and $\rho(r)$ and λ are the correlation function and correlation length, respectively. The size of the flow domain (e.g., the length of a river downstream from $x = 0$) is $L = 20 \text{ km}$, while the correlation length is $\lambda = 200 \text{ m}$.

5. Results and discussion

The subsequent results are presented in terms of the dimensionless quantities defined as follows. Let the deterministic quantities λ and \bar{q}_0 represent a characteristic length scale and a characteristic volumetric flux, respectively. Their ratio defines a characteristic time scale τ ,

$$\tau = \lambda^3 / \bar{q}_0. \quad (23)$$

We introduce dimensionless quantities

$$\tilde{x} = \frac{x}{\lambda}, \quad \tilde{t} = \frac{t}{\tau}, \quad \tilde{Q} = \frac{Q}{\bar{q}_0}, \quad \tilde{q}_{\text{in}} = \frac{q_{\text{in}}}{\bar{q}_0}, \quad \tilde{\gamma} = \frac{\gamma \bar{q}_0^{3/4}}{\lambda^2}, \quad \tilde{P} = \frac{P}{\tau}. \quad (24)$$

In the simulations reported below, we set $\tilde{P} = 1$.

5.1. Monte Carlo simulations (MCS)

We compare our CDF solutions with those obtained via MCS. These MCS consist of 10,000 realizations of mutually-uncorrelated random fields of $s_0(x)$ and $n(x)$ generated at 501 nodes evenly distributed on the interval $[0, L]$, as well as 10,000 realizations of white noise $q'_0(t)$. For each realization of input parameters, a realization of dependent variables, the integral I_γ and raw CDF Π , are computed from (18) and (14), respectively. The resulting 10,000 realizations of I_γ and Π are then used to estimate their PDFs or CDFs.

5.2. Accuracy of CDF solutions

We start by investigating the accuracy of the three alternative approximations—the constant γ approximation (20) (Const), the CLT-based approximation (CLT) and the white noise γ approximation (21) (Delta)—used to compute the PDF of the random integral $I_\gamma(\tilde{x})$ in (18). Fig. 1 exhibits the PDF $p_\gamma(I)$ computed with these approximations and with MCS at three locations, $\tilde{x} = 0.5$, $\tilde{x} = 5$ and $\tilde{x} = 100$. The accuracy of the constant γ approximation degrades with the distance away from the upstream boundary, i.e., as \tilde{x} increases. On the other hand, the accuracy of both the CLT and white-noise approximations improves as \tilde{x} becomes large, with the CLT approximation being the most accurate. Fig. 2 demonstrates the close agreement between the flow-rate CDFs F_q computed with both the CLT approximation-based CDF solution (19) and MCS.

Given the flow rate CDF $F_q(Q)$ in (19), the n -th ensemble moment of the flow rate q is computed as

$$\mu_q \equiv \langle \tilde{q} \rangle = \int_0^\infty [1 - F_q(\tilde{Q})] d\tilde{Q}, \tag{25a}$$

$$\langle (\tilde{q} - \mu_q)^n \rangle = n \int_0^\infty (\tilde{Q} - \mu_q)^{n-1} [1 - F_q(\tilde{Q})] d\tilde{Q} + (-\mu_q)^n, \quad n \geq 2. \tag{25b}$$

Fig. 3 depicts the first two ensemble moments of q , i.e., its mean μ_q and variance σ_q^2 , computed with N realizations of MCS and analytically with (25) at $\tilde{x} = 50$ and $\tilde{t} = 0.0006$. The number of realizations required for MCS to converge increases with the order n of the ensemble moment. The mean flow rate μ_q requires only $N = 300$ realizations to converge, whereas close to $N = 10,000$ realizations are needed for the variance σ_q^2 . Although not shown here, $N = 10,000$ realizations are not enough for MCS to converge to a stable estimate of kurtosis (the third ensemble moment of q).

To elucidate this effect further, we investigate the MCS convergence for the tails of the distribution of q . Let us consider a relative error $\mathcal{E}(Q)$ for the flow-rate CDF $F_q(Q)$ computed with N realizations of MCS (F_q^{MCS}) and the CDF solution (F_q^{CDF}),

$$\mathcal{E}(Q) = \frac{|F_q^{MCS}(Q) - F_q^{CDF}(Q)|}{F_q^{CDF}(Q)} \times 100\%. \tag{26}$$

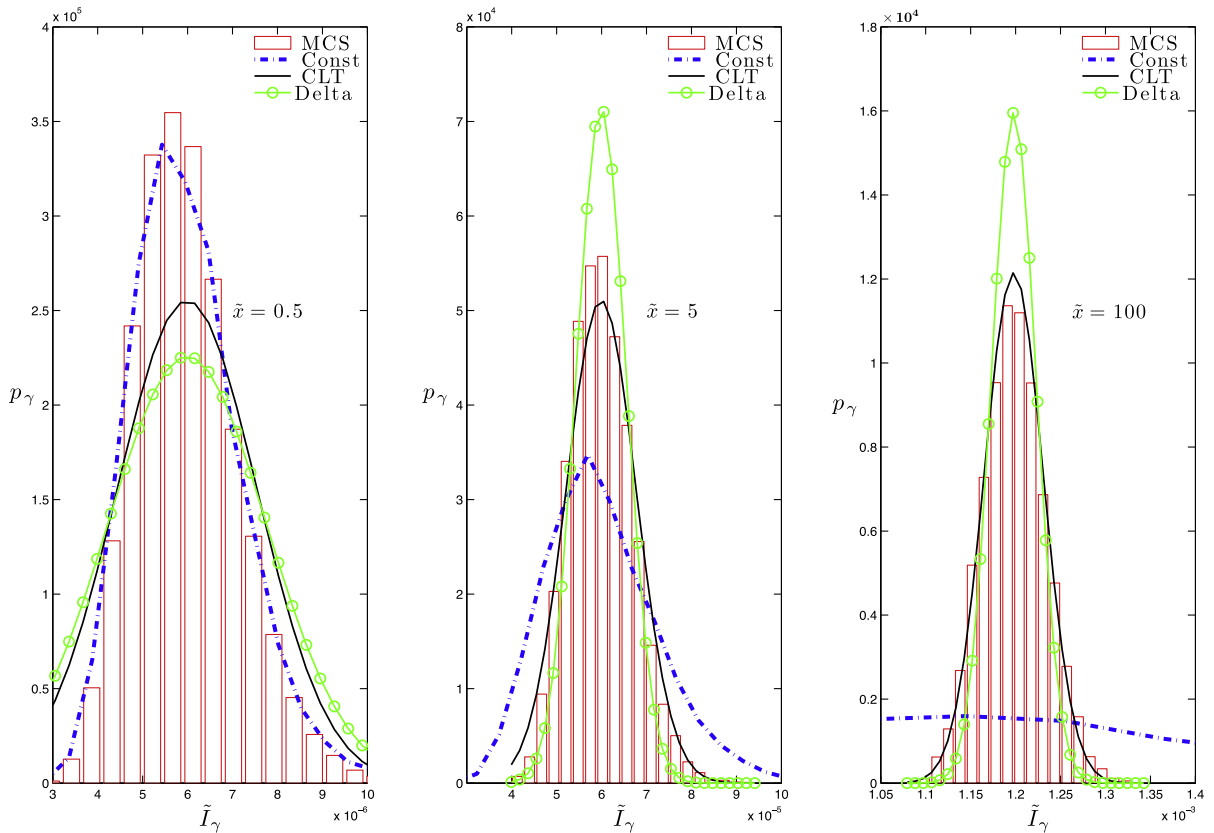


Fig. 1. Random integral, $I_\gamma(x)$, computed with MCS, the constant γ approximation (20) (Const), the CLT-based approximation (CLT) and the white noise γ approximation (21) (Delta).

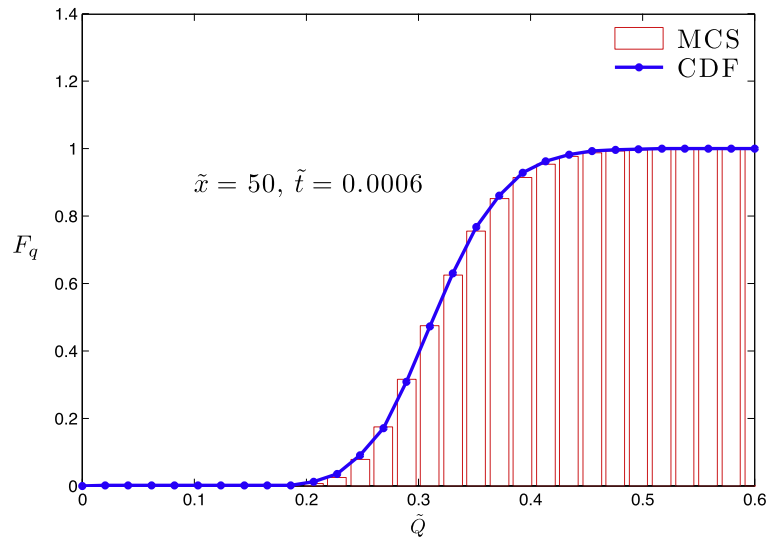


Fig. 2. Flow rate CDF, F_q , computed with MCS and the CDF method at $\bar{x} = 50$ and $\bar{t} = 0.0006$.

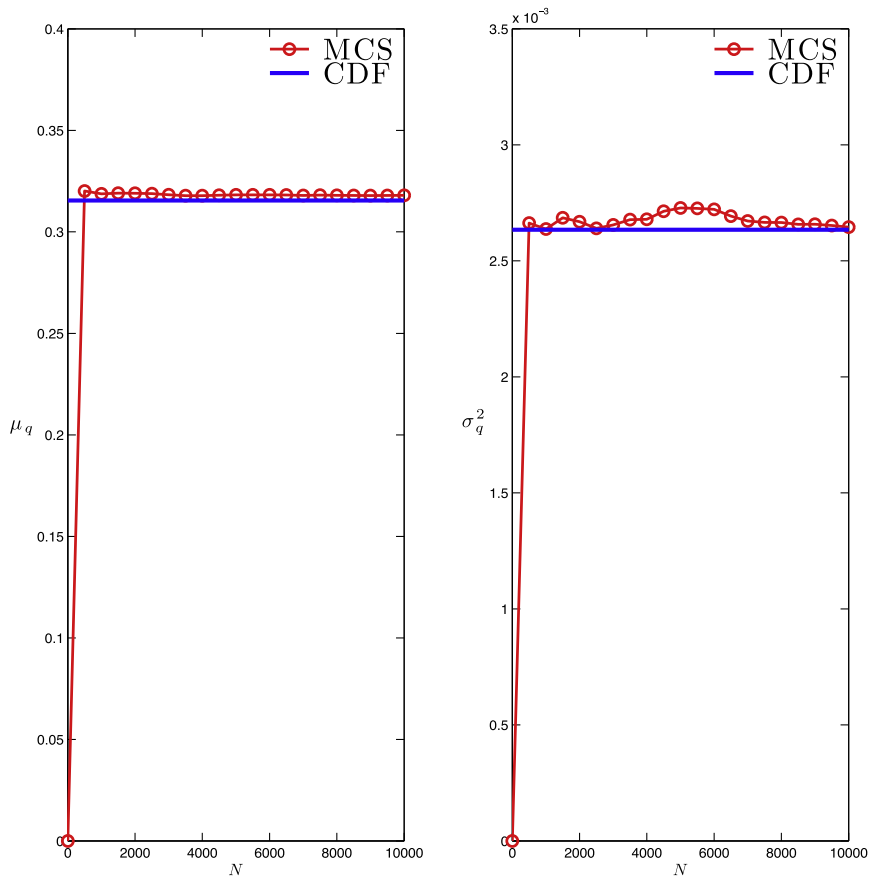


Fig. 3. Mean (μ_q) and variance (σ_q^2) of the flow-rate q computed with the CDF method and with N realizations of MCS at point ($\bar{x} = 50$, $\bar{t} = 0.0006$).

Fig. 4 exhibits the relative error $\mathcal{E}(\bar{Q})$, as a function of the number of MCS realization N , computed at ($\bar{x} = 50$, $\bar{t} = 0.0006$) for $\bar{Q} = 0.3$, 0.4 , and 0.5 . After $N = 10,000$ realizations, $\mathcal{E}(\bar{Q})$ drops from 6% for $\bar{Q} = 0.3$ to almost zero for $\bar{Q} = 0.5$. This finding is to be expected since $F_q(\bar{Q})$ is defined as the probability of (non-negative) flow rate q not exceeding a certain value \bar{Q} ,

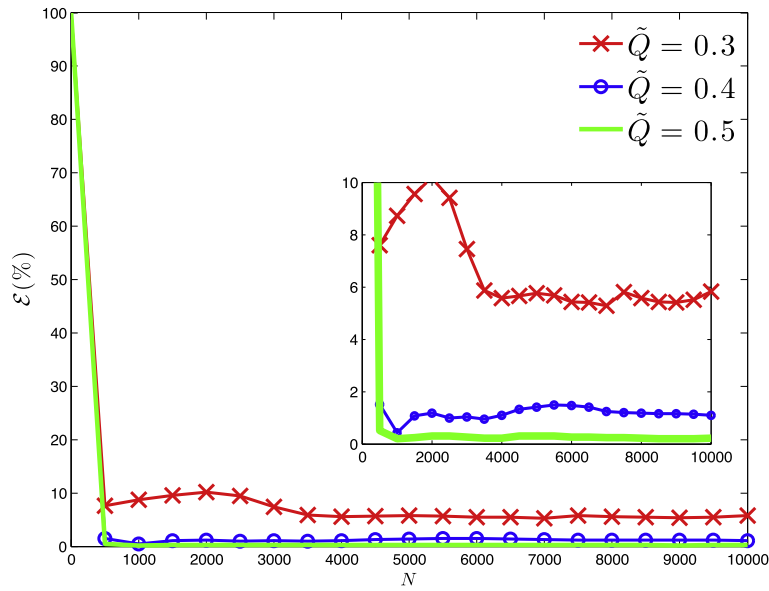


Fig. 4. Relative error $\mathcal{E}(\tilde{Q})$, as a function of the number of MCS realization N , computed at $(\tilde{x} = 50, \tilde{t} = 0.0006)$ for $\tilde{Q} = 0.3, 0.4$, and 0.5 .

i.e., $F_q(\tilde{Q}) \equiv \Pr[\tilde{q} \leq \tilde{Q}]$. Small values of \tilde{Q} (e.g., $\tilde{Q} = 0.3$) represent extreme events, whose low probability requires a large number of realizations N for MCS to converge.

5.3. Temporal evolution of CDF

Fig. 5 shows snapshots of the temporal evolution of the flow-rate CDF $F_q(\tilde{Q}; \tilde{x} = 10, \tilde{t})$ at dimensionless time $\tilde{t} = 0.00001, \tilde{t} = 0.00015$ and $\tilde{t} = 0.001$. At earlier time ($t = 0.00001$), the initial (deterministic) value $\tilde{q}_{in} = 0.5$ corresponds to the CDF given by a step (Heaviside) function. As time increases, upstream fluctuations propagate downstream and reach an observation point ($\tilde{x} = 10$). These fluctuations and parametric uncertainty increase predictive uncertainty of the local flow rate, as demonstrated by $F_q(\tilde{t} = 0.00015)$. At later times ($\tilde{t} = 0.001$), as the wave has passed the observation point, the predictive uncertainty decreases resulting in sharpening F_q which now reflects uncertainty in the upstream boundary fluctuations $q_0^*(t)$ only.

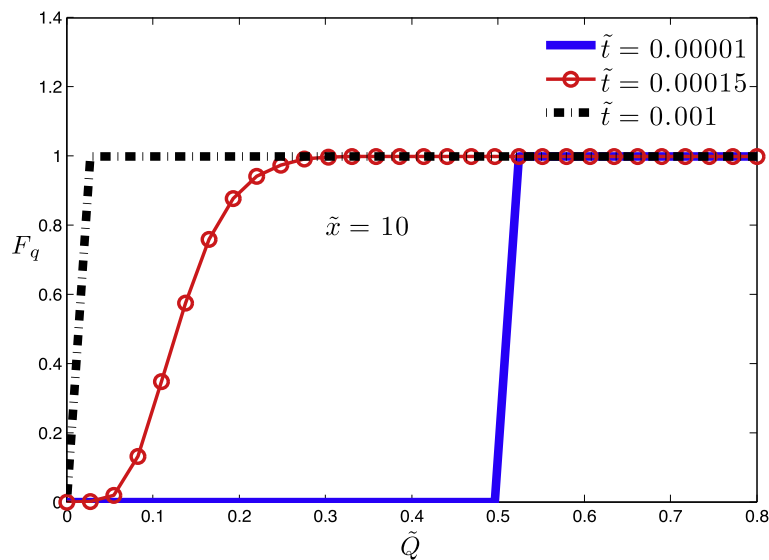


Fig. 5. Snapshots of temporal evolution of the flow-rate CDF, $F_q(\tilde{Q}; \tilde{x}, \tilde{t})$, computed with the CLT-based CDF solution at $\tilde{x} = 10$ and $\tilde{t} = 0.00001, 0.00015$ and 0.001 .

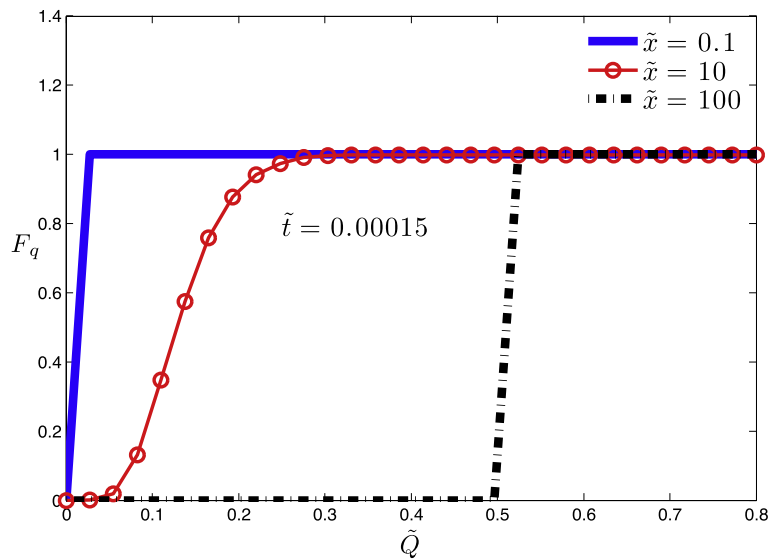


Fig. 6. Spatial evolution of the flow-rate CDF, $F_q(\tilde{Q}; \tilde{x}, \tilde{t})$, computed with the CLT-based CDF solution at $\tilde{t} = 0.00015$ and $\tilde{x} = 0.1, 10$ and 100 .

5.4. Spatial profile of CDF

Fig. 6 exhibits the flow-rate CDF computed for a fixed dimensionless time ($\tilde{t} = 0.00015$) at three locations $\tilde{x} = 0.1, 10$ and 100 . At $\tilde{t} = 0.00015$, the wave has already passed the upstream point $\tilde{x} = 0.1$ and the shape of F_q is dominated by the upstream boundary fluctuation $q'_0(t)$. The wave is located further downstream, where high predictive uncertainty stems from the combined effects of uncertainty in temporal fluctuations $q'_0(t)$ and spatial variability of the system parameter $s_0(x)$ and $n(x)$, as represented by the flow-rate CDF at $\tilde{x} = 10$. Even further downstream ($\tilde{x} = 100$), where the wave is yet to reach, the flow-rate CDF sharpens, reflecting uncertainty in the upstream boundary fluctuations $q'_0(t)$ only.

6. Conclusion

We developed a probabilistic approach to quantify parametric uncertainty in first-order hyperbolic conservation laws (kinematic wave equations). The approach relies on the derivation of a deterministic equation for the cumulative density function (CDF) of the system state, in which probabilistic descriptions (probability density functions or PDFs) of the system parameters and/or initial and boundary conditions serve as inputs. The accuracy and robustness of solutions of the CDF equation for one such system, the Saint–Venant equations of river flows, were investigated via comparison with Monte Carlo simulations. Our analysis leads to the following major conclusions.

1. CDF equations, and their (semi-) analytical solutions, provide a computationally efficient alternative to the existing methods for uncertainty quantification, such as Monte Carlo simulations and stochastic finite element methods (polynomial chaos expansions, stochastic collocation methods, etc.).
2. CDF equations are ideally suited for handling input parameters and/or initial and boundary conditions that exhibit small correlation lengths. This is in contrast with stochastic finite element methods and other numerical approaches that rely on the Karhunen–Loève representation of random parameter fields.
3. CDF equations offer an operational advantage over PDF equations that are often used in other contexts, e.g., to analyze transport of passive tracers and reactive species in turbulent (randomly fluctuating) velocity fields. This is because CDF equations allow for straightforward and unambiguous determination of boundary conditions with respect to sample variables.

The presented analysis relies on the assumption that the relationship $\mathbf{q} = \mathbf{q}(k)$ between a system state $k(\mathbf{x}, t)$ and its flux $\mathbf{q}(\mathbf{x}, t)$ is invertible, which enabled us to treat the flux $\mathbf{q}(\mathbf{x}, t)$ as a primary state variable. However, our CDF approach is equally applicable to hyperbolic conservation laws (1) in which this assumption is invalid and $k(\mathbf{x}, t)$ serves as a primary state variable. A derivation of a corresponding CDF equation for $k(\mathbf{x}, t)$ is outlined in Appendix F.

Acknowledgments

This work was supported by the Applied Mathematics program of the US DOE Office of Advanced Scientific Computing Research.

Appendix A. Statistical properties of γ

The random coefficient $\gamma = (\sqrt{s_0}/n)^{-\beta}$ is defined in terms of the two random parameters, $s_0(x)$ and $n(x)$. Its single-point PDF $p_\gamma(\Gamma; x)$ can be expressed in terms of the PDFs of $s_0(x)$ and $n(x)$ as follows. Let $G_\gamma(\Gamma) = P(\gamma \leq \Gamma)$ denote the cumulative density function of γ , i.e., the probability that the random coefficient γ at point x takes on a value not larger than Γ . By definition,

$$G_\gamma(\Gamma) = \int_0^\infty \int_0^{N(\Gamma, S_0)} p_{n, s_0}(N, S_0) dN dS_0, \tag{A.1}$$

where $p_{n, s_0}(N, S_0)$ is the joint PDF of the channel slope s_0 and the Manning coefficient n at point x . The PDF p_γ can now be obtained as

$$p_\gamma(\Gamma) = \frac{d}{d\Gamma} G_\gamma = \int_0^\infty p_{n, s_0}[N(\Gamma, S_0), S_0] \frac{\partial N(\Gamma, S_0)}{\partial \Gamma} dS_0. \tag{A.2}$$

If s_0 and n are mutually independent, (A.2) reduces to

$$p_\gamma(\Gamma) = \frac{dG_\gamma}{d\Gamma} \frac{1}{\beta} \Gamma^{1/\beta-1} \int_0^\infty p_n[N(\Gamma, S_0)] p_{s_0}(S_0) \sqrt{S_0} dS_0. \tag{A.3}$$

If $Y_1(x) = \ln s_0(x)$ and $Y_2(x) = \ln n(x)$ are mutually uncorrelated multivariate Gaussian stationary (statistically homogeneous) random fields, their two-point PDFs are given by

$$p_{2Y_i}(\xi_1, \xi_2) = \frac{1}{2\pi\sigma_{Y_i}^2 \sqrt{1 - \rho_{Y_i}^2}} \exp\left[-\frac{R_i(\xi_1, \xi_2)}{2\sigma_{Y_i}^2(1 - \rho_{Y_i}^2)}\right], \quad i = 1, 2, \tag{A.4a}$$

where

$$R_i = (\xi_1 - \bar{Y}_i)^2 - 2\rho_{Y_i}(\xi_1 - \bar{Y}_i)(\xi_2 - \bar{Y}_i) + (\xi_2 - \bar{Y}_i)^2 \tag{A.4b}$$

and $\rho_{Y_i}(x_1, x_2)$ denotes the linear correlation function between $Y_i(x_1)$ and $Y_i(x_2)$. The two-point covariance of $\gamma(x)$, $C_\gamma(x_1, x_2) = \langle \gamma(x_1)\gamma(x_2) \rangle$, is defined by

$$C_\gamma(x_1, x_2) = \langle \gamma(x_1)\gamma(x_2) \rangle - \bar{\gamma}^2 = C_1(x_1, x_2)C_2(x_1, x_2) - \bar{\gamma}^2. \tag{A.5}$$

The covariances $C_1(x_1, x_2) = \langle [(s_0(x_1)s_0(x_2))^{-\beta/2}] \rangle$ and $C_2(x_1, x_2) = \langle [n(x_1)n(x_2)]^\beta \rangle$ can be expressed in terms of the statistics of $s_0(x)$ and $n(x)$,

$$C_1(x_1, x_2) = \int_{-\infty}^\infty \int_{-\infty}^\infty e^{-\frac{\beta}{2}(S_1+S_2)} p_{2Y_1}(S_1, S_2) dS_1 dS_2 = e^{-\beta\bar{Y}_1 + \beta^2(1+\rho_{Y_1})\sigma_{Y_1}^2/4} \tag{A.6}$$

and

$$C_2(x_1, x_2) = \int_{-\infty}^\infty \int_{-\infty}^\infty e^{\beta(N_1+N_2)} p_{2Y_2}(N_1, N_2) dN_1 dN_2 = e^{2\beta\bar{Y}_2 + \beta^2(1+\rho_{Y_2})\sigma_{Y_2}^2}. \tag{A.7}$$

Appendix B. Derivation of raw CDF equation

It follows from the definition of Π in (7) that

$$\frac{\partial \Pi}{\partial x} = \frac{\partial \mathcal{H}[Q - q(x, t)]}{\partial x} = \frac{\partial \Pi}{\partial q} \frac{\partial q}{\partial x} = -\frac{\partial \Pi}{\partial Q} \frac{\partial q}{\partial x}. \tag{B.1}$$

Multiplying (4) with $\partial \Pi / \partial Q$ and making use of (B.1) yields

$$\beta\gamma q^{\beta-1} \frac{\partial \Pi}{\partial Q} \frac{\partial q}{\partial t} + \frac{\partial \Pi}{\partial Q} \frac{\partial q}{\partial x} = \frac{\partial \Pi}{\partial Q} S. \tag{B.2}$$

Since $\partial \Pi / \partial Q = \delta(Q - q)$ where $\delta(\cdot)$ is the Dirac delta function, and since for any test function $g(\cdot)$ the following relation holds $g(q)\delta(Q - q) = g(Q)\delta(Q - q)$, one can rewrite (B.2) as

$$\beta\gamma Q^{\beta-1} \frac{\partial \Pi}{\partial Q} \frac{\partial q}{\partial t} - \frac{\partial \Pi}{\partial x} = \frac{\partial \Pi}{\partial Q} S. \tag{B.3}$$

Finally, substituting the relation

$$\frac{\partial \Pi}{\partial t} = \frac{\partial \mathcal{H}[Q - q(x, t)]}{\partial t} = \frac{\partial \Pi}{\partial q} \frac{\partial q}{\partial t} = -\frac{\partial \Pi}{\partial Q} \frac{\partial q}{\partial t}, \tag{B.4}$$

into (B.3) yields an equation for the raw CDF (9).

Appendix C. Solution for $S = 0$

Taking the Laplace transformation of (9) with $S \equiv 0$ yields

$$\frac{d\hat{\Pi}}{dx} + \beta Q^{\beta-1} \gamma s \hat{\Pi} = \beta Q^{\beta-1} \gamma \Pi_{\text{in}}, \quad (\text{C.1})$$

where $\hat{\Pi}(Q; x, s)$ is the Laplace transform of $\Pi(Q; x, t)$. This equation is subject to the boundary condition obtained from (10b),

$$\hat{\Pi}(Q, x = 0, s) = \hat{\Pi}_0 = \int_0^\infty \mathcal{H}[Q - q_0(t)] e^{-st} dt. \quad (\text{C.2})$$

A solution of (C.1) and (C.2) is

$$\hat{\Pi} = \int_0^x e^{-s[C(x)-C(x')] B(x')} dx' + \hat{\Pi}_0 e^{-sC(x)}, \quad (\text{C.3})$$

where

$$B(x) = \beta Q^{\beta-1} \gamma(x) \mathcal{H}[Q - q_{\text{in}}(x)], \quad C(x) = \int_0^x \beta Q^{\beta-1} \gamma(x') dx'. \quad (\text{C.4})$$

The inverse Laplace transform of (C.3) and (C.4) is given by

$$\Pi = \int_0^x \delta[t - C(x) + C(x')] B(x') dx' + \mathcal{H}(t - C) \mathcal{H}[Q - q_0(t - C)]. \quad (\text{C.5})$$

Evaluating the quadrature, while recalling the definitions of B and C in (C.4), yields

$$\Pi = \mathcal{H}[Q - q_{\text{in}}(x^*)] + \mathcal{H}(t - C) \mathcal{H}[Q - q_0(t - C)]. \quad (\text{C.6})$$

Here $x' = x^*$ is a solution of the equation

$$C(x') = C(x) - t \quad (\text{C.7})$$

for a given x and t . It follows from (C.4) that $C(x' = x^*) \geq 0$ for all x and t . This imposes the constraint $C(x) \geq t$ on the parameter space of (C.7), which translates into the Heaviside function $\mathcal{H}(C - t)$ in (14).

Appendix D. Solution for $S = S(x)$

Taking the Laplace transformation of (9), (10) with $S = S(x)$ yields

$$\frac{\partial \hat{\Pi}}{\partial x} + S(x) \frac{\partial \hat{\Pi}}{\partial Q} = -\beta Q^{\beta-1} \gamma(x) (s \hat{\Pi} - \Pi_{\text{in}}), \quad (\text{D.1})$$

subject to the boundary conditions

$$\hat{\Pi}(Q; 0, s) = \hat{\Pi}_0(Q, s), \quad \hat{\Pi}(0; x, s) = 0. \quad (\text{D.2})$$

A family of characteristics $Q = Q(x; \xi)$ is defined by

$$\frac{dQ}{dx} = S(x), \quad Q(x = 0) = \xi, \quad (\text{D.3})$$

which yields an equation for characteristics

$$Q = \int_0^x S dx' + \xi. \quad (\text{D.4})$$

The “label” ξ defines the origin of each characteristic line, such that (see Fig. D.1)

1. for $\xi \geq 0$, characteristics originate from the Q -axis ($x = 0$) and the solution is determined by the boundary condition on x ;
2. for $\xi < 0$, characteristics originate from the x -axis ($x = \eta$) and the solution is determined by the boundary condition on Q .
The constant η is a solution of $\int_0^\eta S dx' = -\xi$.

Along the characteristics (D.4), Eq. (D.1) takes the form

$$\frac{d\hat{\Pi}}{dx} = -\beta Q^{\beta-1} \gamma(x) (s \hat{\Pi} - \Pi_{\text{in}}). \quad (\text{D.5})$$

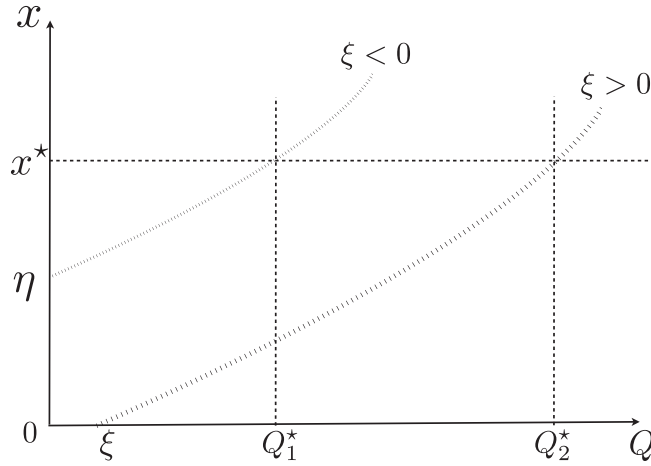


Fig. D.1. Characteristic curves in the (x, Q) plane for $\hat{I}(Q; x, s)$.

The two boundary conditions in (D.2) give rise to the boundary condition for (D.5),

$$\hat{I}(Q; x_0, s) = \hat{I}_0(\xi, s), \quad x_0 = \begin{cases} 0 & \xi \geq 0 \\ \eta & \xi < 0 \end{cases}, \quad \hat{I}_0 = \int_0^\infty \mathcal{H}[\xi - q_0(t)] e^{-st} dt. \tag{D.6}$$

Substituting (D.4) into (D.5), solving the resulting ODE, and eliminating ξ in favor of x and Q in the solution, yields

$$\hat{I} = \int_{x_0}^x e^{-s(C-A)} B dx' + \hat{I}_0(x_0, s) e^{-sC}, \tag{D.7}$$

where

$$A = \int_{x_0}^{x'} \beta [Q - I(x, x'')]^{\beta-1} \gamma dx'', \tag{D.8}$$

$$B = \beta [Q - I(x, x')]^{\beta-1} \gamma \mathcal{H}[Q - I(x, x') - q_{in}(x')], \tag{D.9}$$

$$C = \int_{x_0}^x \beta [Q - I(x, x'')]^{\beta-1} \gamma dx'', \quad I(x, x') = \int_{x'}^x S dx''. \tag{D.10}$$

The inverse Laplace transform of (D.7) and (D.8) is given by

$$\Pi = \int_{x_0}^x \delta(t - C + A) B dx' + \mathcal{H}(t - C) \mathcal{H}[Q - I(x, 0) - q_0(t - C)]. \tag{D.11}$$

Evaluating the quadrature, while recalling the definitions of A, B and C in (D.8), yields

$$\Pi = \mathcal{H}[Q - I(x, x^*) - q_{in}(x^*)] + \mathcal{H}(t - C) \mathcal{H}[Q - I(x, 0) - q_0(t - C)]. \tag{D.12}$$

Here $x' = x^*$ is a solution of the equation

$$A(x, x') = C(x, x') - t \tag{D.13}$$

for a given x and t . It follows from (D.8) that $A(x, x^*) \geq 0$ for all x and t . This imposes the constraint $C(x, x') \geq t$ on the parameter space of (D.13), which translates into the Heaviside function $\mathcal{H}(C - t)$ in (16).

Appendix E. Integration of correlated random fields

For intermediate x , we follow the approach presented in [29] to compute the statistics of the integral $I_\gamma(x)$ in (18). It is briefly reviewed here for completeness. Let us subdivide the integration interval $[0, x]$ into $2N$ intervals of length $\Delta = x/(2N)$. Then (18) can be rewritten as

$$I_\gamma(x) = \sum_{i=1}^N (I_i + J_i), \quad I_i = \int_{(2i-1)\Delta}^{2i\Delta} \gamma(x') dx', \quad J_i = \int_{(2i-2)\Delta}^{(2i-1)\Delta} \gamma(x') dx'. \tag{E.1}$$

Since $\gamma(x)$ is stationary, the integrals I_i and J_i ($i = 1, \dots, N$) have the same mean $\bar{I} = \bar{J} = \bar{\gamma}\Delta$ and variance

$$\sigma_I^2 = \sigma_J^2 = \int_{(2i-1)\Delta}^{2i\Delta} \int_{(2i-1)\Delta}^{2i\Delta} \rho_\gamma(x' - x'') dx' dx'' = 2\sigma_\gamma^2 \int_0^\Delta (\Delta - x) \rho_\gamma(y) dy. \tag{E.2}$$

The correlation coefficient between the two sums is given by

$$\rho_N \left(\sum_{i=1}^N I_i, \sum_{j=1}^N J_j \right) = \frac{2N-1}{2N} \frac{\int_0^\Delta \rho_\gamma(y) dy}{\int_0^\Delta (\Delta-y) \rho_\gamma(y) dy}. \quad (\text{E.3})$$

According to the central limit theorem for dependent processes, $I_\gamma(x) = \sum_{i=1}^N (I_i + J_i)$ is asymptotically (as $N \rightarrow \infty$) Gaussian with mean $2N\bar{I}$ and variance $2N(1 + \rho_N)\sigma_I^2$.

Appendix F. CDF equation for $k(x, t)$

If the constitutive relation $q = q(k)$ in the hyperbolic conservation law (1) is not invertible, one can derive a CDF equation for $k(x, t)$ by redefining the raw CDF as

$$\Pi_k(K; x, t) = \mathcal{H}[K - k(x, t)]. \quad (\text{F.1})$$

When applied to (2) with an arbitrary differentiable $q(k)$, the procedure outlined in Appendix B yields a raw CDF equation

$$\frac{\partial \Pi_k}{\partial t} + q'(K) \frac{\partial \Pi_k}{\partial x} + S(x, t) \frac{\partial \Pi_k}{\partial K} = 0, \quad (\text{F.2})$$

where the prime indicates the derivative of $q(k)$ with respect to k .

Taking the ensemble average of (F.2) and either invoking a closure approximation or using the method of characteristics (both of which are discussed above in the context of the CDF for q), one obtains closed-form deterministic equations for the CDF of k .

The same procedure is applicable to (1) in two or three spatial dimensions.

References

- [1] M.J. Lighthill, G.B. Whitham, On kinematic waves. I. Flood movement in long rivers, Proc. R. Soc. London Ser. A 229 (1178) (1955) 281–316.
- [2] M.J. Lighthill, G.B. Whitham, On kinematic waves. II. A theory of traffic flow on long crowded roads, Proc. R. Soc. London Ser. A 229 (1178) (1955) 317–345.
- [3] V.P. Singh, Kinematic Wave Modeling in Water Resources: Surface Water Hydrology, Wiley, New York, 1996.
- [4] V.P. Singh, Kinematic wave modeling in water resources: a historical perspective, Hydrol. Process. 15 (2001) 671–706.
- [5] R.J. Moore, S.J. Cole, V.A. Bell, D.A. Jones, Issues in flood forecasting: ungauged basins, extreme floods and uncertainty, in: I. Tchiguirinskaia, K.N.N. Thein, P. Hubert (Eds.), Frontiers in Flood Research, International Association of Hydrological Sciences, vol. 305, IAHS Publ., 2006, pp. 103–122.
- [6] P.S. Eagleson, Dynamics of flood frequency, Water Resour. Res. 8 (4) (1972) 878–898.
- [7] M. Kavvas, R.S. Govindaraju, Stochastic overland flows, part 1: Physics-based evolutionary probability distributions, Stoch. Hydrol. Hydraul. 5 (2) (1991) 89–104.
- [8] R.S. Govindaraju, M. Kavvas, Stochastic overland flows, part 2: Numerical solutions evolutionary probability density functions, Stoch. Hydrol. Hydraul. 5 (2) (1991) 105–124.
- [9] M. Kavvas, Nonlinear hydrologic processes: conservation equations for determining their means and probability distributions, J. Hydrol. Eng. 8 (2) (2003) 44–53.
- [10] J. Yoon, M.L. Kavvas, Probabilistic solution to stochastic overland flow equation, J. Hydrol. Eng. 8 (2) (2003) 54–63.
- [11] L. Séguis, B. Cappelaere, C. Peugeot, B. Vieux, Impact on Sahelian runoff of stochastic and elevation-induced spatial distributions of soil parameters, Hydrol. Process. 16 (2) (2002) 313–332.
- [12] R. Morbidelli, C. Corradini, R.S. Govindaraju, A simplified model for estimating field-scale surface runoff hydrographs, Hydrol. Process. 21 (13) (2007) 1772–1779.
- [13] G. Lin, C.-H. Su, G.E. Karniadakis, Predicting shock dynamics in the presence of uncertainties, J. Comput. Phys. 217 (1) (2006) 260V276.
- [14] R. Abgrall, A simple, flexible and generic deterministic approach to uncertainty quantifications in non linear problems: application to fluid flow problems, Tech. rep., Rapport de Recherche INRIA, 2007.
- [15] J. Tryoen, O. Le Maître, M. Ndjing, A. Ern, Intrusive Galerkin methods with upwinding for uncertain nonlinear hyperbolic systems, J. Comput. Phys. 229 (18) (2010) 6485–6511.
- [16] R. Abgrall, P.M. Congedo, C. Corre, S. Galéra, A simple semi-intrusive method for uncertainty quantification of shocked flows, comparison with a non-intrusive polynomial chaos method, in: J.C.F. Pereira, A. Sequeira, J.M.C. Pereira (Eds.), V European Conference on Computational Fluid Dynamics ECCOMAS CFD 2010, Lisbon, Portugal, 2010. ISBN: 978-989-96778-1-4.
- [17] L. Ge, K.F. Cheung, Spectral sampling method for uncertainty propagation in long-wave runup modeling, J. Hydraul. Eng. 137 (3) (2011) 277–288.
- [18] G. Poëtte, B. Després, D. Lucor, Uncertainty propagation for systems of conservation laws, high order stochastic spectral methods, in: J.S. Hesthaven, E.M. Rnquist (Eds.), Spectral and High Order Methods for Partial Differential Equations, Lecture Notes in Computational Science and Engineering, vol. 76, Springer-Verlag, Berlin Heidelberg, 2011, pp. 293–305.
- [19] S.B. Pope, Turbulent Flows, Cambridge University Press, 2000.
- [20] D.M. Tartakovsky, S. Broyda, PDF equations for advective-reactive transport in heterogeneous porous media with uncertain properties, J. Contam. Hydrol. 120–121 (2011) 129–140.
- [21] J.A. Seddon, River hydraulics, Trans. Amer. Soc. Civ. Eng. 43 (1900) 179–243.
- [22] D.L. Buhman, T.K. Gates, C.C. Watson, Stochastic variability of fluvial hydraulic geometry: mississippi and red rivers, J. Hydrol. Eng. 128 (2002) 426–437.
- [23] T.K. Gates, M. Al-Zahrani, Spatiotemporal stochastic open-channel flow. I: Model and its parameter data, J. Hydrol. Eng. 122 (11) (1996) 641–651.
- [24] T.K. Gates, M. Al-Zahrani, Spatiotemporal stochastic open-channel flow. II: Simulation experiments, J. Hydrol. Eng. 122 (11) (1996) 652–661.
- [25] T. Moramarco, V.P. Singh, A practical method for analysis of river waves and for kinematic wave routing in natural channel networks, Hydrol. Process. 14 (2000) 51–62.
- [26] D. Gottlieb, D. Xiu, Galerkin method for wave equations with uncertain coefficients, Commun. Comput. Phys. 3 (2) (2008) 505–518.
- [27] R.H. Kraichnan, Eddy viscosity and diffusivity: exact formulas and approximations, Complex Syst. 1 (1987) 805–820.
- [28] D.M. Tartakovsky, A. Guadagnini, F. Ballio, A.M. Tartakovsky, Localization of mean flow and equivalent transmissivity tensor for bounded randomly heterogeneous aquifers, Transp. Porous Media 49 (1) (2002) 41–58.
- [29] O. Ditlevsen, G. Mohr, P. Hoffmeyer, Integration of non-Gaussian fields, Probab. Eng. Mech. 11 (1996) 15–23.
- [30] L. Liang, M.L. Kavvas, Modeling of solute transport and macrodispersion by unsteady stream flow under uncertain conditions, J. Hydrol. Eng. 13 (6) (2008) 510–520.